Electronic Supporting Information

Qing-Hua Zou [a], Wen-Hao Yang [b], Ling-Kun Wu [a], Lu-Lu Jiang [a], Shuai-Hua Wang [b], Lang Liu [a], Ren-Fu Li [b]*, Heng-Yun Ye [a], Jian-Rong Li [a]*

[a] Chaotic Matter Science Research Center, International Institute for Innovation, Jiangxi University of Science and Technology, Ganzhou 341000, P. R. China.

[b] CAS Key Laboratory of Design and Assembly of Functional Nanostructures, and Fujian Key Laboratory of Nanomaterials, Fujian Institute of Research on the Structure of Matter, Chinese Academy of Sciences, Fuzhou, Fujian 350002, China.

Corresponding authors:

jrli@fjirsm.ac.cn

lirenfu@fjirsm.ac.cn

Experimental section

1.1 Materials

CuI(99.5%), [Bmim]I (99%), (Bmim = 1-butyl-3-methylimidazolium), 1,4-Dimethylpiperazine (98%), DMF (99.8%), reference scintillator $Bi_3Ge_4O_{12}$ (BGO)、$(Lu, Y)_2SiO_5$: Ce^{3+} (LYSO: Ce) purchased from Shanghai Blue Crystal Optoelectronics Technology Co. All reagents and solvents were used directly without further purified.

1.2 Synthesis of Compound 1

A mixture of CuI (1 mmol, 190 mg), 1,4-Dimethylpiperazine (1 mmol, 114 mg) was placed in a Pyrex, and [Bmim]I (1 mmol, 266 mg) was dropped into the bottom of the Pyrex. The Pyrex was sealed after evacuation and headed 100°C for 12 hours. Upon slow cooling of the solution to room temperature over 24 hours, colorless transparency crystals of **1** was obtained by washed with acetonitrile three times. Yield: 48% (based on CuI).

Compound **1**, Anal. (%) calc.: C 14.56, H 2.85, N 5.66. Found (%): C 14.95, H 2.85, N 5.77.

1.3 General Characterizations：

The PXRD of **1** was measured on a Rigaku DMax 2500 powder diffractometer with Cu $K\alpha$ radiation (λ = 1.54178 Å) in the angular range of 2θ = 5 - 55°. Single crystal X-ray diffraction data for **1** was collected on a Rigaku Collaboration diffractometer using Mo-Kα (λ = 0.71073 Å) radiation from a graphite monochromator. All crystal

structure data were solved using the direct method and refined using the full matrix method based on F2 data from the Olex2 software package[1]. Solid-state ultraviolet-visible (UV-Vis) optical absorption spectroscopy was performed on a Shimadzu 2600 UV/Vis spectrophotometer. Thermal stability testing uses thermogravimetric analysis (TGA) on a NETZSCH STA 449F3 thermal analyzer under the continuous protection of N_2 atmosphere flow. C, H and N elementals analysis were carried out on a Perkin-Elmer model 240 C elemental analyzer. Steady-state PL emission and PL excitation (PLE) spectra were measured using a PL spectrometer (FLS980; Edinburgh Instruments). Temperature-dependent steady-state and TRPL spectra were recorded using an FLS980 spectrometer (Edinburgh) equipped with a continuous xenon lamp (450 W), a pulsed flash lamp, a 375 nm picosecond pulsed laser, and a temperature-controlled instrument (Linkam). THMS600). The absolute PLQY of single crystals was measured by using a standard $BaSO_4$-coated integrating sphere (diameter 150 mm, Edinburgh) as the sample chamber mounted on an FLS980 spectrometer.

The X-ray excitation fluorescence spectrometer is homemade, the whole skeleton is based on an FLS920 spectrometer with a PMT (HAMAMATSU R928) detector, the excitation Xe-lamp is replaced by a high purity tungsten target, the X-ray tube voltage is set to 50 kV, and a lead box is used as an X-ray protection device. The RL spectrum of the compound was recorded at room temperature using an FLS920 spectrometer (Edinburgh) equipped with a high-purity tungsten target (5 W). Under X-ray excitation, photons generated by the sample were collected by a photomultiplier tube and converted into a current, the dose rate of which was determined by an X-ray dosimeter.

1.4 Computational Methods.

All calculations using density functional theory (DFT) were carried out using the Vienna Ab initio simulation package (VASP).[2] The generalized gradient approximation of the Perdew−Burke−Ernzerhof (PBE) parametrization with the projector-augmented wave (PAW) method was performed for the exchange and correlation functional.[3, 4] For all elements, including Cu, I, C, N and H, ultrasoft pseudopotentials were used. The kinetic energy cutoff of 420 eV and a 2 × 2 × 1 Monkhorst–Pack k-point mesh for the wave function basis set were employed. The energy convergence criterion is set as 1.0×10^{-5} eV for structural relaxations. Finally, data processing and graphical plotting were performed using Vaspkit and Origin software.

1.5 Calculation of X-ray attenuation coefficient

The X-ray attenuation coefficients of the compound and standard samples were

obtained from the XCOM database provided by the National Institute of Standards and Technology. The absorption was further determined using the Beer-Lambert law, expressed by the following equation:

$$\mathrm{I} = \mathrm{I}_0 e^{-\alpha d}$$

where *I* is the intensity of the transmitted X-ray photons, I_0 is the initial intensity of the X-ray photons, α is the total attenuation coefficient, and *d* is the thickness of the active layer. Then, the attenuation ratio of the active layers with various thicknesses could be obtained as follows:

$$\text{Attenuation ratio} = \frac{\mathrm{I}_0 - \mathrm{I}}{\mathrm{I}_0} = 1 - e^{-\alpha d}$$

1.6 Calculation of Detection limit:

Utilizing X-rays at a low dose rate, a linear relationship between RL intensity and dose was established, with the noise data collected in the absence of the sample. A Gaussian function was employed to fit the noise intensity values, with the FWHM considered as the average noise level. The calculation formula for the limit of detection (LOD) is given by LOD = 3*FWHM/k, where the signal-to-noise ratio is set at 3, and k represents the slope of the linear fitting curve.[5]

Equation S1： Utilizing the commercial scintillator BGO (8000 photons/MeV) and LYSO: Ce (33200 photons/MeV) as references, the light yield of $Cu_4I_4(C_6H_{14}N_2)_2$ was estimated by comparing the integrated area of its RL emission spectrum to that of the standard sample. To minimize experimental errors, the powdered samples were pressed into solid cubes before testing, and then cut to prepare test blocks with dimensions (5 mm × 5 mm × 1 mm) matching those of the standard sample. The RL spectra were acquired under identical voltage and current conditions (50 kV, 100 μA), The X-ray outlet was set to 1 cm away from sample for all spectral measurement, and the estimation was subsequently performed using the following formula. Furthermore, the spectral corrections (e.g., sensibility, wavelength and absorption coefficience) were also considered for the scintillation light yield calculation.

$$\frac{\mathrm{LY}_{\mathrm{sample}}}{\mathrm{LY}_{\mathrm{LYSO:\,Ce/BGO}}} = \frac{R_{\mathrm{sample}}}{R_{\mathrm{LYSO:\,Ce/BGO}}} \times \frac{\int I_{\mathrm{LYSO:\,Ce/BGO}}(\lambda)/\mathrm{S}(\lambda) \int I_{\mathrm{LYSO:\,Ce/BGO}}(\lambda)\mathrm{d}\lambda}{\int I_{\mathrm{sample}}(\lambda)/\mathrm{S}(\lambda) \int I_{\mathrm{sample}}(\lambda)\mathrm{d}\lambda}$$

where R is defined as the X-ray deposited energy percentage of scintillators, $I(\lambda)$ is the radioluminescence spectrum at different wavelengths, and $S(\lambda)$ represents the detection efficiency at different irradiation area, respectively.

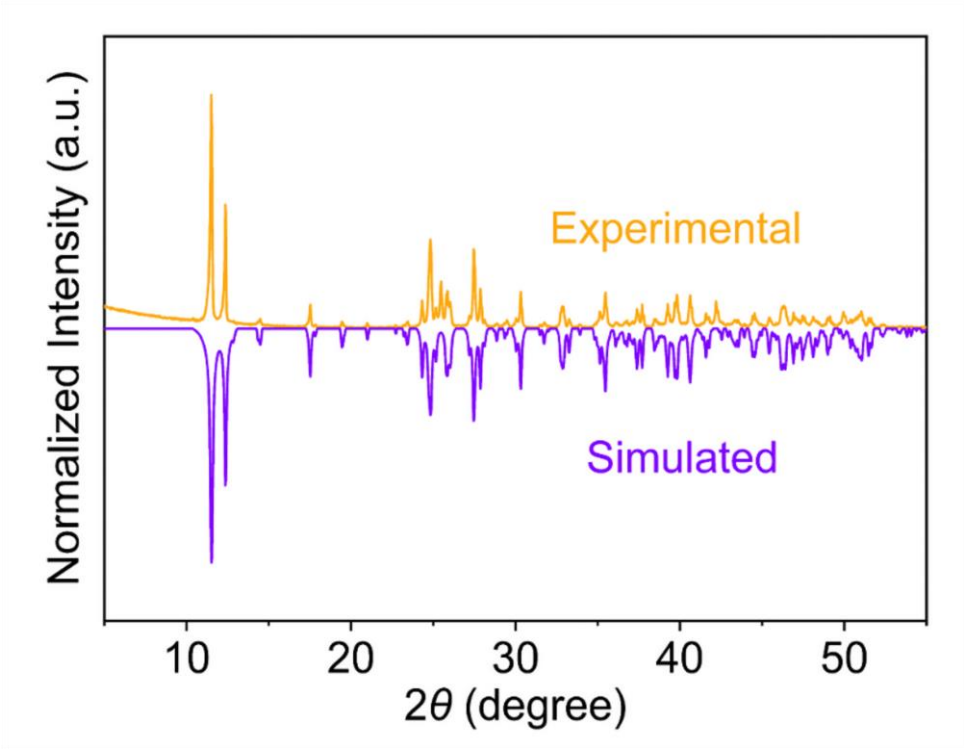

Fig. S1 Experimental and simulated PXRD patterns of **1-CH_3CN.**

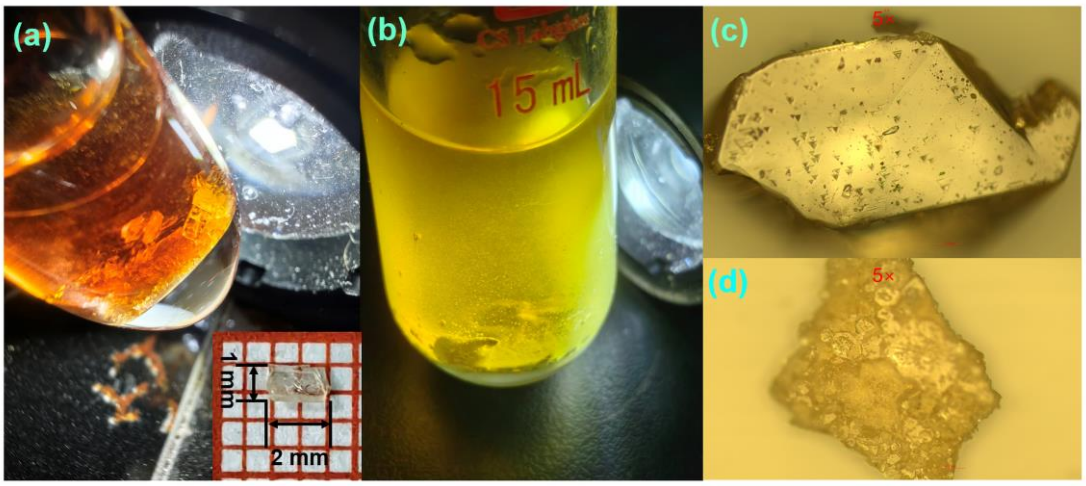

Fig. S2 (a) The crystal photo of **1** synthesized in [Bmim]I. inset: a single crystal picture. (b) The crystal photo of **1-CH_3CN** synthesized in CH_3CN. The surface of as-synthesized samples observed by magnified 5 times under a polarized light microscope (c) single crystal of **1** synthesized in [Bmim]I and (d) **1-CH_3CN** synthesized in CH_3CN.

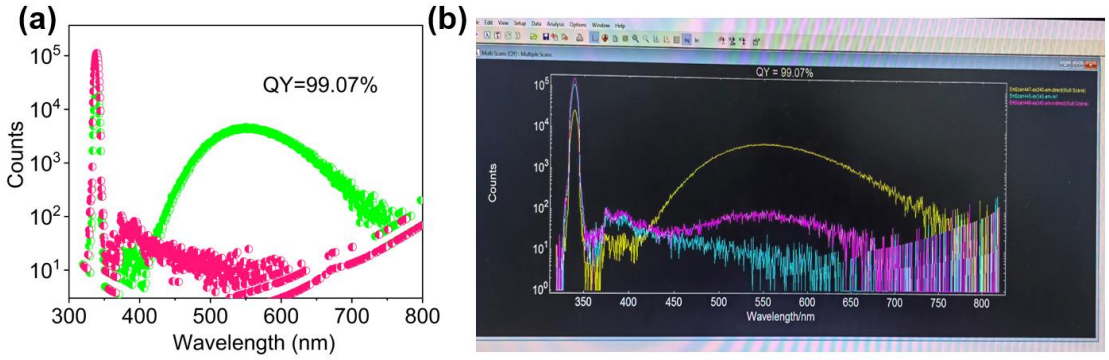

Fig. S3 The PLQY spectrum of **1** (a) and (b).

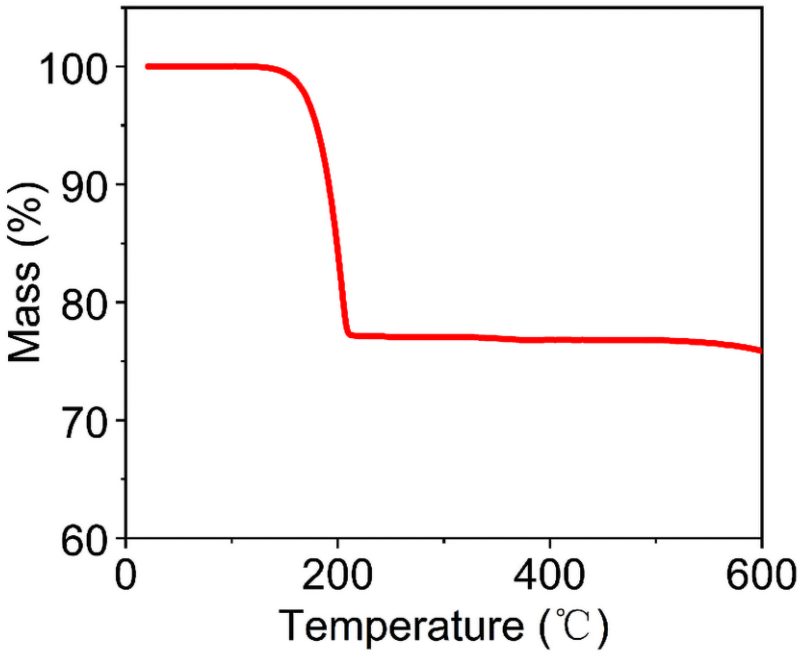

Fig. S4 Thermogravimetric (TGA) curve of **1**.

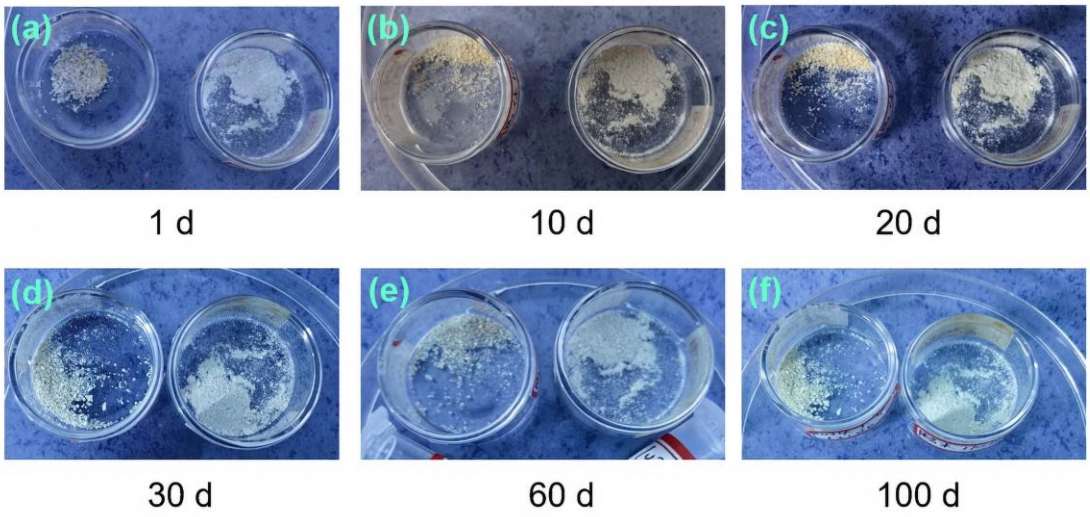

Fig. S5 (a)-(f): Photos of **1** exposed to air at different time.

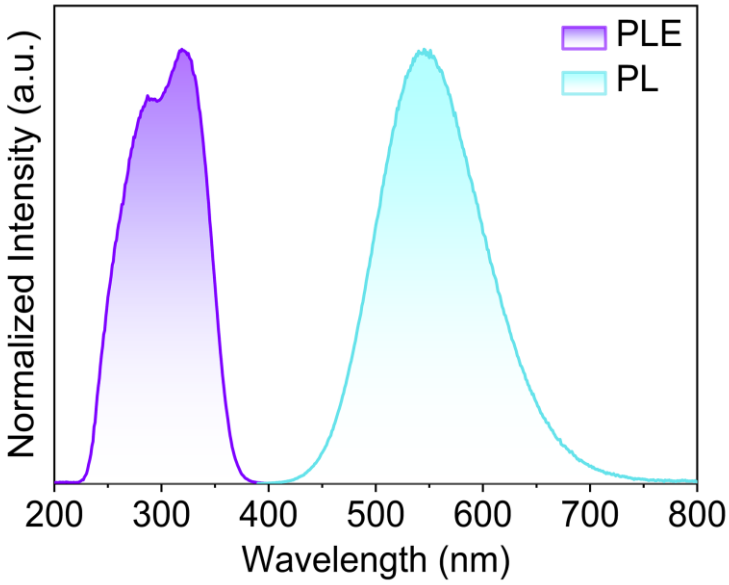

Fig. S6 PLE and PL spectra of **1-CH_3CN**.

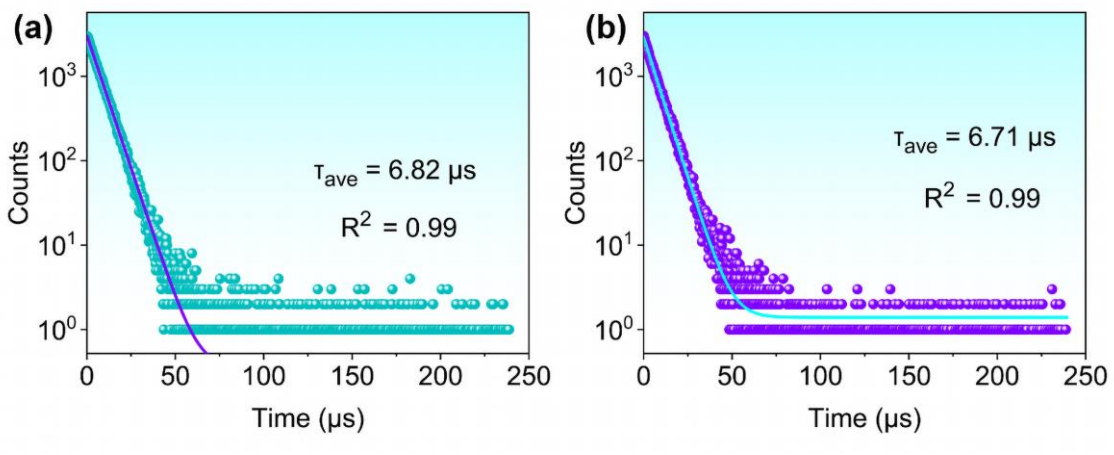

Fig. S7 (a) Lifetime decay curves of **1-100d**. (b) Lifetime decay curves of **1-CH_3CN.**

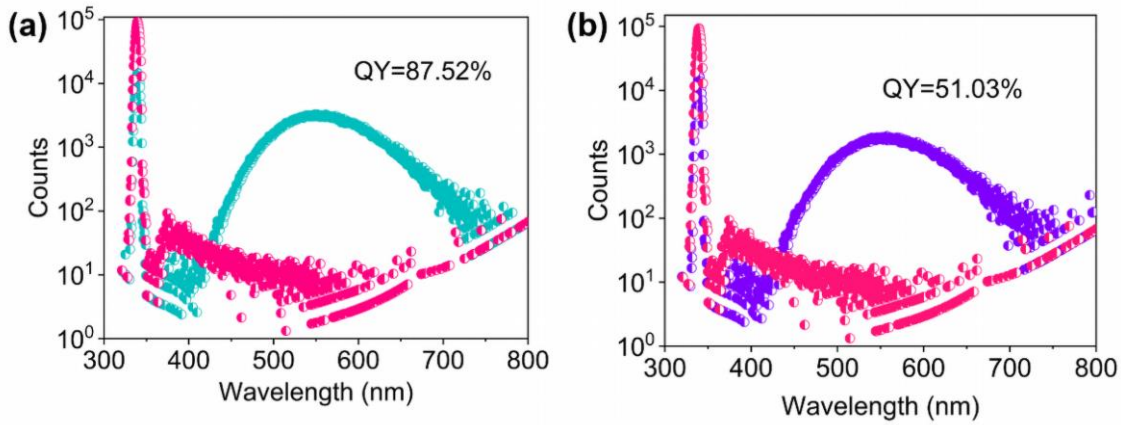

Fig. S8 (a) The PLQY spectrum of **1-100d**. (b) The PLQY spectrum of **1-CH_3CN.**

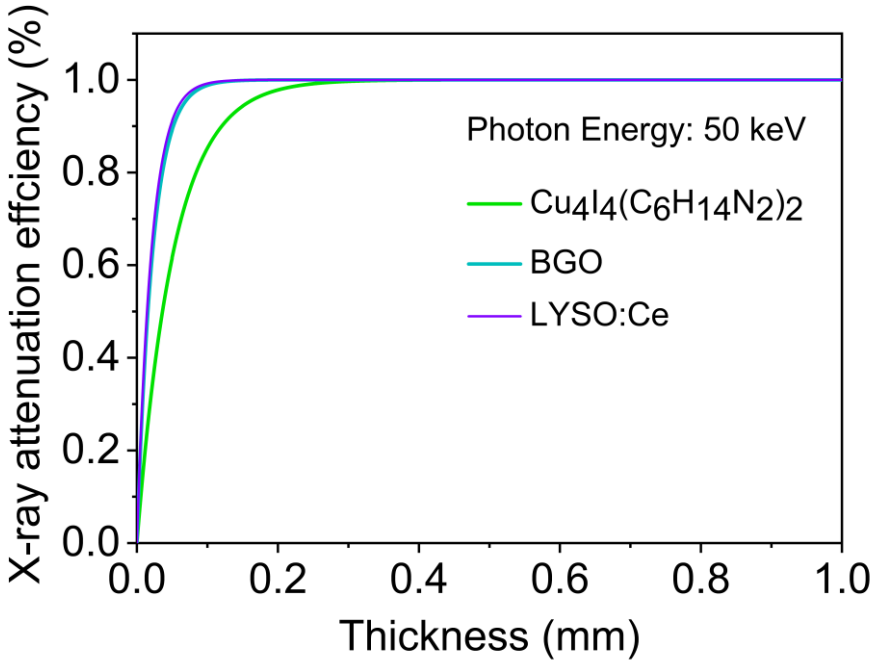

Fig. S9 The curve of the attenuation efficiency versus thickness for **1**, BGO, and LYSO: Ce.

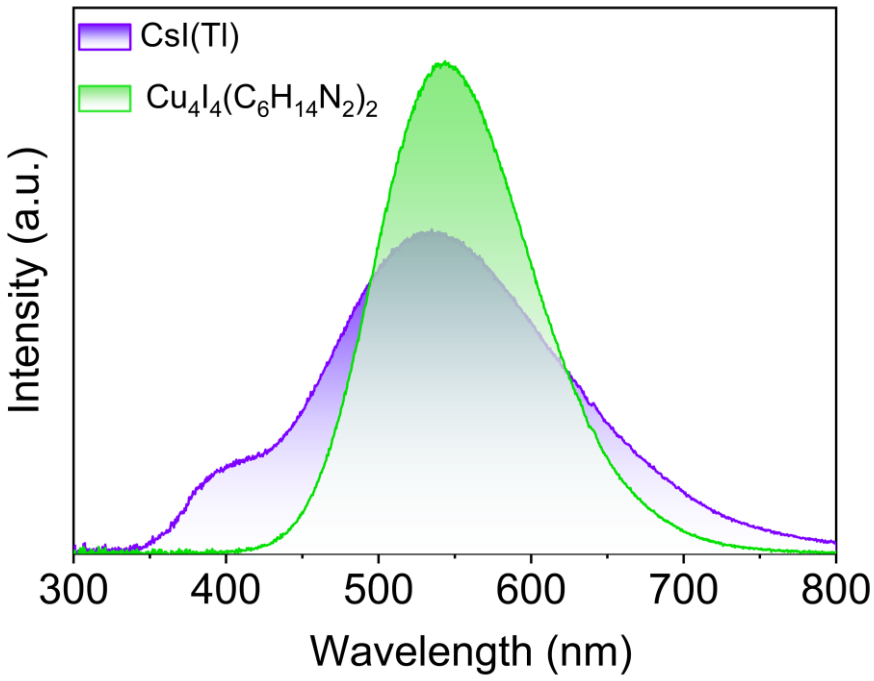

Fig. S10 The RL spectra of **1** and CsI(Tl) under the excitation of X-ray (50 kV, 100 μA).

Table S1 Crystal structure and refinement detail of **1**.

	$Cu_4I_4(C_6H_{14}N_2)_2$
T / K	300
Formula weight	990.14
Crystal system	monoclinic
Space group	*I*2/a
a / Å	14.3126(4)
b / Å	14.3125(4)
c / Å	23.5910(7)
α / °	90
β / °	90.331(2)
γ / °	90
V / Å^3	4832.5(2)
Z	8
D_{calc} / g·cm^{-3}	2.722
μ / mm^{-1}	8.587
F(000)	3648
2θ range / °	4.024-61.952
Reflns collected	25082
Independent refunds (R_{int})	5987(0.0384)
No. of parameters	221
R_1[a], wR_2[b] [I>2σ(I)]	0.0342,0.0714
R_1, wR_2 [all data]	0.0474,0.0756
GOF	1.121
$\Delta\rho$[c] / e·Å^{-3}	0.87/-1.10
CCDC	2388111

[a] $R_1 = \Sigma||F_o|-|F_c||/|F_o|$; [b] $wR_2 = [\Sigma w(F_o^2-F_c^2)^2]/\Sigma w(F_o^2)^2]^{1/2}$; [c] maximum and minimum residual electron density.

Table S2 Bond lengths [Å] for compound **1** at 300 K.

Compound 1			
I1-Cu1	2.7192(8)	I4-Cu4	2.7073(9)
I1-Cu3	2.6912(9)	Cu1-Cu2	2.6997(11)
I1-Cu4	2.7120(9)	Cu1-Cu3	3.0337(10)
I2-Cu1	2.6803(9)	Cu1-Cu4	2.8593(11)
I2-Cu2	2.7227(9)	Cu1-N1	2.149(5)
I2-Cu4	2.6753(8)	Cu2-Cu3	2.8642(10)
I3-Cu1	2.6873(9)	Cu2-Cu4	2.9883(10)
I3-Cu2	2.6943(9)	Cu2-N2	2.146(5)
I3-Cu3	2.7111(8)	Cu3-Cu4	2.6934(11)
I4-Cu2	2.6659(8)	Cu3-N3	2.139(5)
I4-Cu3	2.6676(9)	Cu4-N4	2.144(5)

Table S3 Angles [°] for compound **1** at 300 K.

Compound 1			
Cu3-I1-Cu1	68.21(2)	N1-Cu1-Cu4	150.65(15)
Cu3-I1-Cu4	59.80(2)	I2-Cu2-Cu3	105.49(3)
Cu4-I1-Cu1	63.53(2)	I2-Cu2-Cu4	55.63(2)
Cu1-I2-Cu2	59.95(2)	I3-Cu2-I2	117.72(3)
Cu4-I2-Cu1	64.54(2)	I3-Cu2-Cu1	59.76(2)
Cu4-I2-Cu2	67.22(2)	I3-Cu2-Cu3	58.29(2)
Cu1-I3-Cu2	60.22(2)	I3-Cu2-Cu4	102.01(3)
Cu1-I3-Cu3	68.38(2)	I4-Cu2-I2	101.51(3)
Cu2-I3-Cu3	63.99(2)	I4-Cu2-I3	110.84(3)
Cu2-I4-Cu3	64.96(2)	I4-Cu2-Cu1	114.43(3)
Cu2-I4-Cu4	67.57(2)	I4-Cu2-Cu3	57.55(2)
Cu3-I4-Cu4	60.14(2)	I4-Cu2-Cu4	56.87(2)
I1-Cu1-Cu3	55.46(2)	Cu1-Cu2-I2	59.25(2)
I1-Cu1-Cu4	58.11(2)	Cu1-Cu2-Cu3	66.01(3)
I2-Cu1-I1	110.74(3)	Cu1-Cu2-Cu4	60.10(3)
I2-Cu1-I3	119.49(3)	Cu3-Cu2-Cu4	54.75(2)
I2-Cu1-Cu2	60.80(3)	N2-Cu2-I2	121.18(15)
I2-Cu1-Cu3	102.05(3)	N2-Cu2-I3	100.50(15)

I2-Cu1-Cu4	57.65(2)	N2-Cu2-I4	104.46(14)
I3-Cu1-I1	99.89(3)	N2-Cu2-Cu1	143.26(14)
I3-Cu1-Cu2	60.02(3)	N2-Cu2-Cu3	132.99(15)
I3-Cu1-Cu3	56.18(2)	N2-Cu2-Cu4	154.94(15)
I3-Cu1-Cu4	105.64(3)	I1-Cu3-I3	99.99(3)
Cu2-Cu1-I1	110.01(3)	I1-Cu3-Cu1	56.33(2)
Cu2-Cu1-Cu3	59.60(3)	I1-Cu3-Cu2	106.04(3)
Cu2-Cu1-Cu4	64.96(3)	I1-Cu3-Cu4	60.48(3)
Cu4-Cu1-Cu3	54.30(2)	I3-Cu3-Cu1	55.44(2)
N1-Cu1-I1	124.51(13)	I3-Cu3-Cu2	57.72(2)
N1-Cu1-I2	100.87(14)	I4-Cu3-I1	119.80(3)
N1-Cu1-I3	102.52(14)	I4-Cu3-I3	110.27(3)
N1-Cu1-Cu2	125.21(13)	I4-Cu3-Cu1	101.89(3)
N1-Cu1-Cu3	154.62(14)	I4-Cu3-Cu2	57.49(2)
I4-Cu3-Cu4	60.66(3)	I2-Cu4-Cu2	57.15(2)
Cu2-Cu3-Cu1	54.39(2)	I2-Cu4-Cu3	111.88(3)
Cu4-Cu3-I3	109.75(3)	I4-Cu4-I1	117.63(3)
Cu4-Cu3-Cu1	59.55(3)	I4-Cu4-Cu1	105.54(3)
Cu4-Cu3-Cu2	64.97(3)	I4-Cu4-Cu2	55.55(2)
N3-Cu3-I1	103.87(14)	Cu1-Cu4-Cu2	54.94(3)
N3-Cu3-I3	123.88(13)	Cu3-Cu4-I1	59.72(2)
N3-Cu3-I4	100.35(14)	Cu3-Cu4-I4	59.20(2)
N3-Cu3-Cu1	155.58(15)	Cu3-Cu4-Cu1	66.15(3)
N3-Cu3-Cu2	149.08(15)	Cu3-Cu4-Cu2	60.28(3)
N3-Cu3-Cu4	126.26(13)	N4-Cu4-I1	100.43(15)
I1-Cu4-I1	58.35(2)	N4-Cu4-I2	105.04(14)
I1-Cu4-Cu2	102.19(3)	N4-Cu4-I4	120.47(15)
I2-Cu4-I1	111.12(3)	N4-Cu4-Cu1	133.72(15)
I2-Cu4-I4	101.67(3)	N4-Cu4-Cu2	155.28(15)
I2-Cu4-Cu1	57.82(2)	N4-Cu4-Cu3	142.34(14)

Table S4 Temperature-dependent crystallographic data of compound **1**.

$Cu_4I_4(C_6H_{14}N_2)_2$	**100 K**	**150 K**	**200 K**	**250 K**	**300 K**
Formula weight	990.14	990.14	990.14	990.14	990.14
Crystal system	monoclinic	monoclinic	monoclinic	monoclinic	monoclinic
Space group	*I*2/*a*	*I*2/*a*	*I*2/*a*	*I*2/*a*	*I*2/a
a / Å	14.2370(5)	14.2557(5)	14.2776(4)	14.2979(4)	14.3126(4)
b / Å	14.2608(4)	14.2740(5)	14.2859(4)	14.2985(4)	14.3125(4)
c / Å	23.3211(7)	23.3764(8)	23.4378(6)	23.5008(6)	23.5910(7)
α / °	90	90	90	90	90
β / °	90.525(3)	90.489(3)	90.435(3)	90.400(2)	90.331(2)
γ / °	90	90	90	90	90
V / $Å^3$	4734.7(3)	4756.6(3)	4780.4(2)	4804.4(2)	4832.5(2)
Z	8	8	8	8	8
D_{calc} / $g·cm^{-3}$	2.778	2.765	2.752	2.738	2.722
μ / mm^{-1}	8.765	8.725	8.681	8.638	8.587
F(000)	3648.0	3648.0	3648.0	3648.0	3648
2*θ range* / °	4.042-61.732	4.038-61.62	4.034-61.644	4.028-61.87	4.024-61.952
Reflns collected	14954	14952	14998	16423	25082
Independent refunds (R_{int})	5963(0.0439)	5959(0.0331)	5988(0.0393)	6106(0.0259)	5987(0.0384)
No. of parameters	221	221	221	221	221
R_1[a], wR_2[b] [$I>2\sigma(I)$]	0.0339, 0.0654	0.0337, 0.0670	0.0324, 0.0689	0.0327, 0.0693	0.0342,0.0714
R_1, wR_2 [all data]	0.0450, 0.0678	0.0425, 0.0693	0.0424, 0.0706	0.0399, 0.0709	0.0474,0.0756
GOF	1.135	1.125	1.176	1.205	1.121
$\Delta\rho$[c] / $e·Å^{-3}$	1.39/-1.27	1.18/-1.15	1.07/-1.01	0.87/-0.83	0.87/-1.10

[a] $R_1 = \Sigma||F_o|-|F_c||/|F_o|$; [b] $wR_2 = [\Sigma w(F_o^2-F_c^2)^2]/\Sigma w(F_o^2)^2]^{1/2}$; [c] maximum and minimum residual electron density.

Table S5 Cluster center bond length data for compound **1** from 100 K to 300 K.

	100 K	150 K	200 K	250 K	300 K
Cu1···Cu2	2.6607(9)	2.6692(10)	2.6802(10)	2.6902(10)	2.6997(11)
Cu1···Cu3	2.9788(9)	2.9903(9)	3.0034(12)	3.0164(9)	3.0337(10)
Cu1···Cu4	2.7992(9)	2.8126(9)	2.8262(10)	2.8415(10)	2.8593(11)
Cu2···Cu3	2.8018(10)	2.8134(10)	2.8303(10)	2.8449(10)	2.8642(10)
Cu2···Cu4	2.9255(10)	2.9388(10)	2.9549(10)	2.9706(10)	2.9883(10)
Cu3···Cu4	2.6565(9)	2.6641(10)	2.6736(10)	2.6828(10)	2.6934(11)
I1-Cu1	2.6897(8)	2.6952(8)	2.7013(8)	2.7081(8)	2.7192(8)
I1-Cu3	2.6913(8)	2.6921(8)	2.6927(8)	2.6929(8)	2.6912(9)
I1-Cu4	2.7053(8)	2.7064(8)	2.7089(8)	2.7105(8)	2.7120(9)
I2-Cu1	2.6782(8)	2.6793(8)	2.6795(8)	2.6803(8)	2.6803(9)
I2-Cu2	2.7057(8)	2.7098(8)	2.7131(8)	2.7174(8)	2.7227(9)
I2-Cu4	2.6681(7)	2.6710(7)	2.6710(8)	2.6731(8)	2.6753(8)
I3-Cu1	2.6900(8)	2.6905(8)	2.6900(8)	2.6900(8)	2.6873(9)
I3-Cu2	2.6890(8)	2.6906(8)	2.6920(8)	2.6936(8)	2.6943(9)
I3-Cu3	2.6864(8)	2.6909(8)	2.6965(8)	2.7015(8)	2.7111(8)
I4-Cu2	2.6613(7)	2.6627(7)	2.6636(8)	2.6645(8)	2.6659(8)
I4-Cu3	2.6629(8)	2.6639(8)	2.6654(8)	2.6669(8)	2.6676(9)
I4-Cu4	2.6915(7)	2.6949(8)	2.6989(8)	2.7031(8)	2.7073(8)

Table S6 Comparison of the optical data for **1, 1-CH$_3$CN**, and **1-100d**.

	1	**1-100d**	**1-CH$_3$CN**
Fits (μs)	6.2	6.82	6.71
PL (nm)	544	540	545
FHMW (nm)	109	112	114
Stokes shift (nm)	204	200	205
PLQY (%)	99.07	87.52	51.03
CIE	(0.3686, 0.5349)	(0.359, 0.527)	(0.369, 0.526)

Table S7 Summary of the PL properties and scintillation performance of organic-inorganic hybrid cuprous halides.

Compound	Dimensionality	Emission (nm)	PLQY (%)	light yield (photons/ MeV)	Ref.
$[BAPMA]Cu_2Br_5$	0-D	526	53.4	43744	[6]
$C_9H_{20}NCuBrI$	0-D	464	99.5	25000	[7]
$(R, S\text{-}2\text{-}mpip)_2Cu_2I_6$	0-D	520	65.96	47000	[8]
$[BzTPP]_2Cu_2I_4$	0-D	529	44.2	27706	[9]
$[ETPP]CuBr_2$	0-D	533	65.17	57974	[10]
$[ETPP]_2Cu_4Br_6$	0-D	570	94.15	53576	[10]
$(Bmpip)_2Cu_2Br_4$	0-D	620	48.2	16000	[11]
$(PPh_4)CuBr_2$	0-D	538	1.3	5000	[11]
$ETPA_2Cu_2I_4$	0-D	490	97.56	19900	[12]
$(TPP)_2Cu_4I_6{\cdot}2DMSO$	0-D	515	99.5	—	[13]
$(MTPP)_2CuI_3$	0-D	502	81.95	38750	[14]
$(MTPP)_2Cu_4I_6$	0-D	612	99.7	63700	[14]
$[TBA]_2CuCl_2$	0-D	510	92.8	24134	[15]
$[TBA]_2CuBr_2$	0-D	498	80.5	23373	[15]
$(DIET)_3Cu_3Br_3$	0-D	515	69.2	20700	[16]
$(DIET)_3Cu_3Cl_3$	0-D	530	39.3	6000	[16]
$Cu_4I_4(bzpy)_4$	0-D	573	97	36900	[17]
$Cu_4I_4(tbpy)_4$	0-D	623	91.4	30800	[17]
$[APCHA]Cu_2I_4$	1-D	498	74.8	28336	[18]
$(CuI)_4(C_6H_{14}N_2)_2$	3-D	544	99.07	48538	This work

BAPMA = N,N-Bis(3-aminopropyl) methylamine; mpip = methylpiperazinium; BzTPP = Benzyltriphenylphosphonium; ETPP=Ethyltriphenylphosphonium; Bmpip = 1-butyl-1-methylpiperidinium; PPh_4 = tetraphenylphosphonium; ETPA = ethyltripropylammonium; TPP = tetraphenylphosphonium; MTPP = Methyltriphenylphosphonium; TBA = tetrabutylammonium; DIET = 1,3-Diethyl-2-thiourea; bzpy = 4-benzylpyridine; tbpy = 4-tert-butylpyridine; APCHA = N-(3-aminopropyl)cyclohexylamine.

1. O. V. Dolomanov, L. J. Bourhis, R. J. Gildea, J. A. Howard and H. Puschmann, OLEX2: a complete structure solution, refinement and analysis program, *J. Appl. Crystallogr.*, 2009, **42**, 339-341.
2. G. Kresse and J. Furthmüller, Efficient iterative schemes for ab initio total-energy calculations using a plane-wave basis set, *Phys. Rev. B*, 1996, **54**, 11169.
3. J. P. Perdew, K. Burke and M. Ernzerhof, Generalized gradient approximation made simple, *Phys. Rev. Lett.*, 1996, **77**, 3865.
4. P. E. Blöchl, Projector augmented-wave method, *Phys. Rev. B*, 1994, **50**, 17953.
5. X. Ou, X. Qin, B. Huang, J. Zan, Q. Wu, Z. Hong, L. Xie, H. Bian, Z. Yi and X. Chen, High-resolution X-ray luminescence extension imaging, *Nature*, 2021, **590**, 410-415.
6. Y.-H. Liu, N.-N. Wang, M.-P. Ren, X. Yan, Y.-F. Wu, C.-Y. Yue and X.-W. Lei, Zero-dimensional hybrid cuprous halide of [BAPMA]Cu_2Br_5 as a highly efficient light emitter and an X-ray scintillator, *ACS Appl. Mater. Interfaces* 2023, **15**, 20219-20227.
7. P. Mao, Y. Tang, B. Wang, D. Fan and Y. Wang, Organic-inorganic hybrid cuprous halide scintillators for flexible X-ray imaging, *ACS Appl. Mater. Interfaces* 2022, **14**, 22295-22301.
8. Z. Song, Z. Jia, X. Guo, B. Yu, G. Liu, L. Meng, Y. Liu, Q. Lin and Y. Dang, Chirality–racemization strategy toward copper (I) iodide hybrid single‐crystalline scintillators for X‐ray detection and imaging applications, *Adv. Opt. Mater.* , 2023, **11**, 2203014.
9. N. Lin, R. C. Wang, S. Y. Zhang, Z. H. Lin, X. Y. Chen, Z. N. Li, X. W. Lei, Y. Y. Wang and C. Y. Yue, 0D Hybrid Cuprous Halide as an Efficient Light Emitter and X‐Ray Scintillator, *Laser Photonics Rev.*, 2023, **17**, 2300427.
10. D.-Y. Li, J.-H. Wu, X.-Y. Wang, X.-Y. Zhang, C.-Y. Yue and X.-W. Lei, Reversible triple-mode photo- and radioluminescence and nonlinear optical switching in highly efficient 0D hybrid cuprous halides, *Chem. Mater.*, 2023, **35**, 6598-6611.
11. T. Xu, Y. Li, M. Nikl, R. Kucerkova, Z. Zhou, J. Chen, Y.-Y. Sun, G. Niu, J. Tang and Q. Wang, Lead-free zero-dimensional organic-copper (I) halides as stable and sensitive X-ray scintillators, *ACS Appl. Mater. Interfaces* 2022, **14**, 14157-14164.
12. Y. Zhan, P. Cai, X. Pu, Q. Ai, J. Si, X. Yao, G. Bai and Z. J. I. C. F. Liu, Exceptional optical performance of the zero-dimensional hybrid cuprous halide ETPA2Cu2I4 as an X-ray scintillator, *Inorg. Chem. Front.* , 2024, **11**, 579-588.
13. K. Chen, B. Chen, L. Xie, X. Li, X. Chen, N. Lv, K. Zheng, Z. Liu, H. Pi and Z. Lin, Organic‐Inorganic Copper Halide Compound with a Near‐Unity Emission: Large‐Scale Synthesis and Diverse Light‐Emitting Applications, *Adv. Funct. Mater.*, 2024, **34**, 2310561.
14. S. Cao, J. a. Lai, Y. Wang, K. An, T. Jiang, M. Wu, P. Feng, P. He and X. Tang, Organic‐Inorganic Cuprous Halides With Reversible Photoluminescence for Multiple Optical Applications, *Laser Photonics Rev.* , 2024, 2400799.
15. L. Lian, X. Wang, P. Zhang, J. Zhu, X. Zhang, J. Gao, S. Wang, G. Liang, D. Zhang and L. Gao, Highly luminescent zero-dimensional organic copper halides for X-ray scintillation, *J. Phys. Chem. Lett.*, 2021, **12**, 6919-6926.
16. K. Han, J. Jin, B. Su, J. Qiao and Z. Xia, Promoting Single Channel Photon Emission in Copper (I) Halide Clusters for X‐Ray Detection, *Adv. Opt. Mater.* , 2022, **10**, 2200865.
17. Y. Zhou, T. He, P. Yuan, J. Yin, S. Chen, L. Gutiérrez-Arzaluz, L. Wang, O. M. Bakr and O. F. Mohammed, Colloidal Cu4I4 Clusters for High-Resolution X-ray Imaging Scintillation Screens, *ACS Mater. Lett.*, 2023, **5**, 2002-2008.
18. Z. Gong, J. Zhang, Y.-Y. Liu, L.-X. Zhang, Q. Zhang, L. Xiao, B. Cao, B. Hu and X.-W. Lei, One-

dimensional hybrid copper halides with high-efficiency photoluminescence as scintillator, *Chem. Commun.*, 2024, **60**, 10528-10531.